Phylogenetic differences in calcium permeability of the auditory hair cell cholinergic nicotinic receptor

Marcela Lipovsek[a], Gi Jung Im[b], Lucía F. Franchini[a], Francisco Pisciottano[a], Eleonora Katz[a,c], Paul Albert Fuchs[b], and Ana Belén Elgoyhen[a,d,1]

[a]Instituto de Investigaciones en Ingeniería Genética y Biología Molecular, Consejo Nacional de Investigaciones Científicas y Técnicas, 1428 Buenos Aires, Argentina; [b]Department of Otolaryngology and Head and Neck Surgery and Center for Hearing and Balance, The Johns Hopkins University School of Medicine, Baltimore, MD 21205; [c]Departamento de Fisiología, Biología Molecular y Celular, Facultad de Ciencias Exactas y Naturales, Universidad de Buenos Aires, 1428 Buenos Aires, Argentina; and [d]Departamento de Farmacología, Facultad de Medicina, Universidad de Buenos Aires, 1121 Buenos Aires, Argentina

Edited* by A. J. Hudspeth, Howard Hughes Medical Institute, New York, NY, and approved February 2, 2012 (received for review September 23, 2011)

The α9 and α10 cholinergic nicotinic receptor subunits assemble to form the receptor that mediates efferent inhibition of hair cell function within the auditory sensory organ, a mechanism thought to modulate the dynamic range of hearing. In contrast to all nicotinic receptors, which serve excitatory neurotransmission, the activation of α9α10 produces hyperpolarization of hair cells. An evolutionary analysis has shown that the α10 subunit exhibits signatures of positive selection only along the mammalian lineage, strongly suggesting the acquisition of a unique function. To establish whether mammalian α9α10 receptors have acquired distinct functional properties as a consequence of this evolutionary pressure, we compared the properties of rat and chicken recombinant and native α9α10 receptors. Our main finding in the present work is that, in contrast to the high (pCa^{2+}/pMonovalents ~10) Ca^{2+} permeability reported for rat α9α10 receptors, recombinant and native chicken α9α10 receptors have a much lower permeability (~2) to this cation, comparable to that of neuronal α4β2 receptors. Moreover, we show that, in contrast to α10, α7 as well as α4 and β2 nicotinic subunits are under purifying selection in vertebrates, consistent with the conserved Ca^{2+} permeability reported across species. These results have important consequences for the activation of signaling cascades that lead to hyperpolarization of hair cells after α9α10 gating at the cholinergic–hair cell synapse. In addition, they suggest that high Ca^{2+} permeability of the α9α10 cholinergic nicotinic receptor might have evolved together with other features that have given the mammalian ear an expanded high-frequency sensitivity.

evolution | ionotropic receptor | ligand-gated channel | outer hair cell

Nicotinic cholinergic receptors (nAChRs) are transmembrane allosteric proteins involved in the physiological responses to the neurotransmitter acetylcholine (ACh) (1). They are assembled from five identical (homopentamer) or different (heteropentamer) polypeptide chains arranged symmetrically around a central axis that lines a channel pore (1). The selective pressures for maintaining a wide diversity of nAChR subunits remain unknown (2, 3). The pentameric structure and function of muscle nAChR is well established; however, although much progress has been achieved, the possible combinatorial assemblies of neuronal subunits and their stoichiometry, distribution and function in the central nervous system remain subjects of ongoing investigation (4). Uniquely among these nonmuscle nAChRs, a clear function has been identified for the α9 and α10 nAChR subunits. These subunits assemble to form a pentameric receptor with a likely $\alpha9_2\alpha10_3$ stoichiometry, which serves cholinergic neurotransmission at the synapse between efferent fibers and hair cells of the auditory and vestibular end organs (5–8). Efferent function has been studied in cochlear hair cells, where it is thought to inhibit outer hair cell (OHC) electromotility and so reduce cochlear amplification (9). In contrast to all of the nicotinic receptors that serve excitatory neurotransmission, the activation of α9α10 nAChRs produces hyperpolarization of hair cells (see ref. 9 for a review). This is thought to be produced by entry of Ca^{2+} through the receptor and the subsequent activation of a small-conductance SK2 Ca^{2+}-dependent potassium channel (10, 11). Thus, Ca^{2+} plays a major role in downstream signaling after activation of the α9α10 nAChR.

Analyzing the evolutionary history of α9 and α10 confers an additional degree of complexity to the diversity of nAChRs. Whereas α9 has been under purifying selection (i.e., selection against nonsynonymous substitutions at the DNA level) across all vertebrate species, α10 shows signatures of positive Darwinian selection only along the mammalian lineage (12). This observation suggests the possible acquisition of distinct functional properties for this receptor in mammals. To determine whether mammalian α9α10 nAChRs differ functionally from their nonmammalian vertebrate counterparts, we compared responses mediated by receptors of *Rattus novergicus* (rn, rat) with those of *Gallus gallus* (gg, chicken). We report that, in contrast to the high Ca^{2+} permeability reported for the recombinant and native rat and recombinant human α9α10 receptors (10, 13, 14), recombinant and native chicken α9α10 nAChRs have a much lower permeability to this cation, comparable to that of neuronal α4β2 receptors (15). These results have important physiological implications for the signaling cascades after α9α10 activation at the cholinergic–cochlear hair cell synapse and suggest that the high Ca^{2+} permeability of this nAChR might have accompanied the acquisition of high-frequency sensitivity in mammals.

Results

Responses to ACh. To determine whether chicken α9 and α10 nAChR subunits assemble into functional channels, we injected in vitro transcribed cRNAs into *Xenopus laevis* oocytes and recorded responses to ACh under two-electrode voltage clamp. Injected oocytes responded to ACh in a concentration-dependent manner, with an apparent affinity similar to that of rat receptors (EC_{50}: rn, 12.6 ± 2.0 μM, $n = 6$; gg, 11.0 ± 3.3 μM, $n = 6$; $P = 0.6831$) (Fig. S1*A*). The desensitization kinetics of chicken and rat receptors were similar (Fig. S1*B*).

Calcium Permeability. Rat and human recombinant α9α10 nAChRs (13, 14), as well as native α9α10 nAChRs of rat cochlear hair cells (10), have a high Ca^{2+} permeability [relative Ca^{2+} to monovalent permeability (pCa/pMono) close to or exceeding 10]. Moreover, the fractional Ca^{2+} current (P_f, the fractional Ca^{2+} current, estimated as Ca^{2+} fluorescence increase/total charge entering the cell) in rat α9α10- transfected GH4C1 cells (22%) is the largest

Author contributions: M.L., L.F.F., E.K., P.A.F., and A.B.E. designed research; M.L. and G.J.I. performed research; M.L., F.P., E.K., P.A.F., and A.B.E. analyzed data; and P.A.F. and A.B.E. wrote the paper.

The authors declare no conflict of interest.

*This Direct Submission article had a prearranged editor.

[1]To whom correspondence should be addressed. E-mail: abelgoyhen@gmail.com.

This article contains supporting information online at www.pnas.org/lookup/suppl/doi:10.1073/pnas.1115488109/-/DCSupplemental.

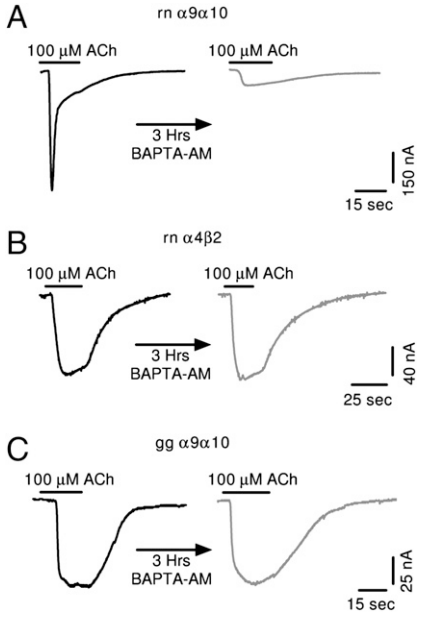

Fig. 1. Chicken α9α10 nAChRs do not activate oocyte $I\mathrm{Cl}_{Ca}$. Representative traces of responses evoked by a 20-s application of 100 μM ACh in oocytes expressing rat α9α10 (*A*), rat α4β2 (*B*), or chicken α9α10 nAChR (*C*), before (*Left*) and after (*Right*) a 3-h incubation with the fast calcium chelator BAPTA-AM (V_{hold} = −70 mV).

value estimated to date for a ligand-gated ion channel (16). To assess the significance of Ca^{2+} flux through chicken recombinant α9α10 nAChRs, in a first set of experiments we analyzed the contribution of the $I\mathrm{Cl}_{Ca}$ to ACh-evoked responses. $I\mathrm{Cl}_{Ca}$ is an endogenous Cl^- current present in *Xenopus* oocytes that is activated by an increase in intracellular Ca^{2+} (17). Receptors with very high Ca^{2+} permeability, such as α7 (18) and α9α10 (7) nAChRs, have a more prominent contribution of the $I\mathrm{Cl}_{Ca}$ to ACh-evoked responses compared with the modest contribution of receptors with lower Ca^{2+} permeability (19). Fig. 1 shows representative responses to 100 μM ACh at a V_{hold} of −70 mV before and after a 3-h incubation with the membrane permeant fast Ca^{2+} chelator 1,2-bis(2-aminophenoxy)ethane-*N,N,N′,N′*-tetraacetic acid-acetoxymethyl ester (BAPTA-AM) for rat α9α10 nAChRs (Fig. 1*A*) and α4β2 nAChRs (Fig. 1*B*), receptors with high (pCa/pMono, 9; ref, 13) and low (pCa/pNa, 1.6; ref. 15) Ca^{2+} permeability, respectively. Whereas ACh-evoked currents were markedly reduced after BAPTA-AM incubation in the case of rat α9α10 receptors (indicating a strong contribution of $I\mathrm{Cl}_{Ca}$ and thus influx of Ca^{2+} through the receptor), the response in α4β2 receptors remained unaffected. A similar experiment performed for chicken α9α10 receptors produced results strikingly similar to those obtained with rat α4β2, but not rat α9α10, nAChRs (Fig. 1*C*). The percentage of remaining response was close to 100% for both chicken α9α10 (100.3% ± 14%; n = 7) and α4β2 (95.7% ± 3.4%; n = 5) receptors, and was 11.7% ± 2.7% (n = 10) for rat α9α10 receptors.

To further estimate the relative Ca^{2+} to monovalent permeability of chicken α9α10 receptors, we evaluated the shift in the reversal potential E_{rev} as a function of increases in extracellular Ca^{2+} concentration as for rat (13) and human (14) α9α10 nAChRs. Current-voltage (I-V) curves were elicited by a 2-s voltage ramp protocol (−120 to +50 mV) at the plateau of the response to ACh from a V_{hold} of −70 mV in the presence of different Ca^{2+} concentrations. Fig. 2*A* shows representative I-V curves for only three Ca^{2+} concentrations for the sake of clarity; insets show a magnification near the E_{rev}. Fig. 2*B* shows averaged E_{rev} as a function of five external Ca^{2+} concentrations. Rat α9α10 receptors demonstrated a significant shift in E_{rev} to more depolarized potentials in response to each increase in extracellular Ca^{2+}. A 10-fold increase in Ca^{2+} concentration from 0.2 to 2 mM resulted in a shift in E_{rev} of 40 ± 8.6 mV (n = 5) (Table S1). Moreover, the fit of the data to a straight line had a slope of 39.3 ± 0.4 (n = 5), which was significantly different from 0 (P = 0.0001), thus illustrating the high degree of dependency of E_{rev} on the extracellular Ca^{2+} concentration. In contrast, the shifts in reversal potential were negligible in the case of rat α4β2 and chicken α9α10 nAChRs (Table S1).

The fit of the foregoing data to the extended Goldman–Hodgkin–Katz (GHK) equation resulted in a pCa/pMono of 10.3 ± 0.9 (n = 5) for rat α9α10 receptors, a result similar to that reported previously (13). In the case of chicken α4β2 and α9α10 receptors, the data from most oocytes did not fit the GHK equation, because of the insensitivity of E_{rev} to variations in extracellular Ca^{2+}

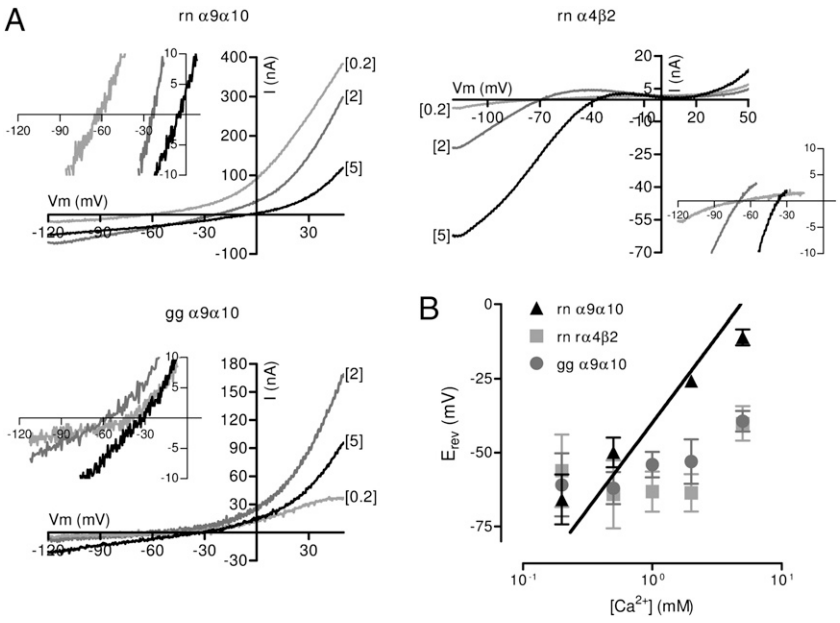

Fig. 2. Chicken recombinant α9α10 nAChR has lower relative calcium permeability. (*A*) Representative I-V curves obtained on application of voltage ramps (−120 to +50 mV, 2 s) at the plateau of the response to 10 μM (α9α10) or 100 μM (α4β2) ACh in oocytes superfused with *N*-methyl glucamine–based solutions containing different Ca^{2+} concentrations for oocytes expressing rat α9α10 (*Upper Left*), rat α4β2 (*Upper Right*), or chicken α9α10 nAChRs (*Lower Left*). (*Insets*) Magnification near the E_{rev}. (*B*) Plots of E_{rev} values as a function of Ca^{2+} concentration for rat α9α10, rat α4β2, and chicken α9α10 nAChRs. Values are mean ± SEM of n = 5–8 per point.

Table 1. Likelihood value estimates for the branch-site and null hypothesis models

	CHRNA4	*CHRNB2*	*CHRNA7*	*CHRNA10*
Foreground lineage: mammals				
LnL H_A	−19,249.50	−12,662.16	−16,620.05	−16,185.80
LnL H_0	−19,250.54	−12,662.16	−16,621.27	−16,190.49
LRT	2.07	0	2.43	9.39
P (χ^2_1)	0.150	1	0.119	0.002
Foreground lineage: placental mammals				
LnL H_A	−19,251.48	−12,662.20	−16,615.01	−16,213.78
LnL H_0	−19,251.48	−12,662.20	−16,616.83	−16,214.76
LRT	0	0	3.64	1.96
P (χ^2_1)	1	1	0.057	0.162
Foreground lineage: birds/reptiles				
LnL H_A	−19,251.48	−12,660.13	−16,621.28	−16,218.23
LnL H_0	−19,251.48	−12,661.07	−16,621.28	−16,218.22
LRT	0	1.90	0	0
P (χ^2_1)	1	0.169	1	1

CHRNA4, *CHRNB2*, *CHRNA7*, and *CHRNA10* genes from 23 vertebrate species described in Table S2 were analyzed using the branch-site test for positive evolution. The analysis was conducted separately three times for each gene, using mammals, placental mammals and birds/reptiles as the foreground lineage. LRT = 2 × (LnLH_A − LnLH_0). H_A, branch-site model; H_0, null hypothesis; LnL, log-likelihood.

concentration. Nonetheless, a fit was possible in three of eight oocytes expressing chicken α9α10 and in one of five oocytes expressing α4β2, for a pCa/pMono value close to 2. In summary, Ca^{2+} permeability of the chicken α9α10 nAChR is similar to that of the heteromeric neuronal α4β2 receptor and significantly lower than that of the rat α9α10 receptor.

Calcium Permeability of nAChRs in Chicken Hair Cells. Earlier studies suggested that Ca^{2+} can permeate the chicken hair cell nAChR (20), but did not define permeability ratios. Tight-seal intracellular recordings were made from "short" hair cells in a region corresponding to ∼500–1,000 Hz along the tonotopically organized basilar papilla from late-stage chicken embryos (days 17–20 in ovo, hatching at day 21). These cells responded to ACh with a combination of ligand-gated cation current followed by Ca^{2+}-dependent potassium current through apamin-sensitive ("SK-like") potassium channels, as demonstrated previously (21).

The isolated ACh current through the α9α10 nAChR was measured as described in *SI Materials and Methods*. Under these conditions, application of ACh (1 mM) from a "puffer" pipette evoked an inward current at negative membrane potentials (Fig. S2*A*), which reversed in sign near 0 mV (Fig. S2 *B* and *C* for step and ramp protocols, respectively). The overall shape of the I-V curves obtained in chicken short hair cells was similar to that reported for rat inner hair cells and OHCs (10, 22).

To estimate the relative pCa/pMono of native chicken α9α10 receptors, we measured the reversal potential of ACh-evoked membrane current in five external Ca^{2+} concentrations ranging from 0.1 to 10 mM. Fig. 3*A* shows representative I-V curves at three Ca^{2+} concentrations, and Fig. 3*B* shows the E_{rev} as a function of external Ca^{2+}. Because each individual I-V curve represents a different chicken short hair cell, the absolute magnitude of responses at different Ca^{2+} concentrations cannot be compared. As the external calcium concentration was increased, the reversal potential shifted to more positive membrane potentials. The variation of E_{rev} with log external Ca^{2+} concentration was fit (minimum least squared difference) with a straight line of slope 5 mV/$\log_{10}[Ca^{2+}]_o$ (n = 5–8 cells at each concentration) (Fig. 3*B*). From the extended GHK equation, the Ca^{2+} permeability relative to that of the dominant monovalent cation was calculated as 2.6. For the purpose of comparison, E_{rev} obtained from rat inner hair cells

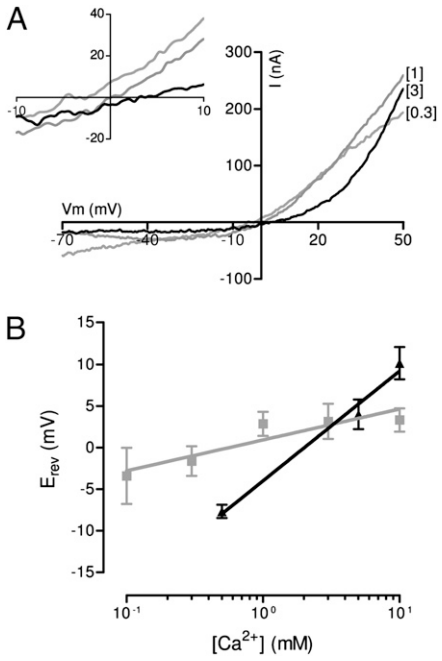

Fig. 3. Chicken short hair cell nAChR has lower relative calcium permeability. (*A*) Representative I-V curves obtained by voltage ramp protocols used to define the reversal potentials in external calcium concentrations of 0.1, 1, and 3 mM. (*Inset*) Magnification near the E_{rev}. Each I-V curve represents a different hair cell, and thus absolute amplitudes cannot be compared. (*B*) Average (± SEM) E_{rev} as a function of external calcium concentration in chicken short hair cells (gray squares, 5–8 cells per point) compared with previously published data for rat inner hair cells (black triangles). (From ref. 9.)

under similar recording conditions (10) are plotted on the same graph. The reversal potential of ACh-evoked currents of rat inner hair cells had a steeper slope (17 mV/$\log_{10}[Ca^{2+}]_o$) (Fig. 3*B*), and a calculated pCa/pMono of 8 (10).

These differences in calcium permeability might influence the subsequent activation of calcium-dependent potassium channels that hyperpolarize and thus inhibit auditory hair cells (10, 21). This question is further complicated by the specialized ultrastructure of the efferent synapse. A near-membrane postsynaptic cistern (23, 24) delimits a restricted diffusion space for ACh-evoked calcium signals and may operate as a source of additional calcium, as a fixed calcium buffer, or both. We examined this possibility using a combination of membrane voltage commands and a "calcium store inhibitor" to alter the ACh-evoked, calcium-dependent potassium current of inner hair cells from the immature rat cochlea and short hair cells of the chicken basilar papilla. ACh (100 μM, 300 ms) was "puff"-applied to rat and chicken hair cells voltage-clamped to −40 mV using ionic conditions to activate calcium-dependent potassium currents in the hair cells (5 mM internal EGTA, 1.3 mM external calcium) (Fig. 4). Near the peak of the evoked outward calcium-dependent potassium current, the membrane potential was then clamped to +40 mV to sharply reduce driving force for inward calcium flux (Fig. 4). As a result, ACh-activated potassium current decayed, reflecting its dependence on calcium influx, but did so at different rates in rat and chicken hair cells (Fig. 4 *A* and *B*). The average ± SEM decay time constant was 37 ± 5 ms in 12 rat inner hair cells and threefold longer, 124 ± 14 ms, in 12 chicken hair cells. Although various factors might influence the decay of ACh-activated potassium current, we uncovered a contribution from synaptic calcium stores by exposing hair cells to the sarcoplasmic/endoplasmic calcium ATPase (SERCA) inhibitor tert-benzo-hydroquinone (t-BHQ;

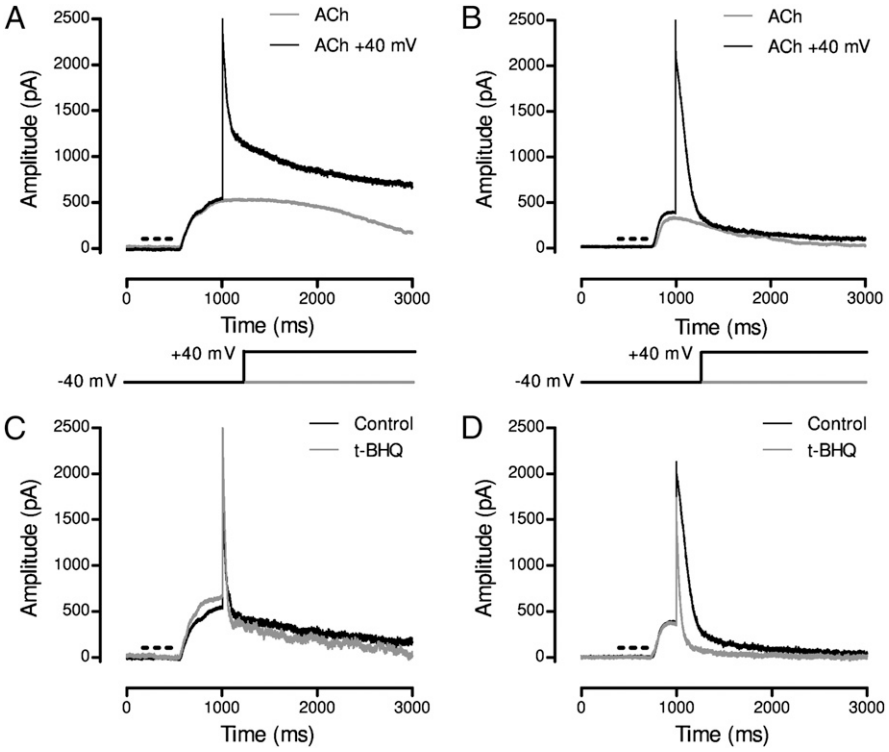

Fig. 4. ACh-evoked potassium current in chicken and rat hair cells. (*A*) A puff of ACh (100 μM for 300 ms) caused an outward current at −40 mV lasting approximately 2 s in rat inner hair cells (gray). When the membrane potential was stepped to +40 mV, the initially large outward current rapidly decayed (black) to a level dominated by a voltage-dependent outward current. (*B*) ACh-evoked membrane current in a chicken hair cell lasting approximately 2 s at −40 mV (gray). With a step to +40 mV, the initially large outward current decayed, albeit relatively slowly, to a level reflecting the small voltage-dependent outward current (black). (*C*) ACh-evoked "difference current" after subtracting membrane current in the absence of ACh in a rat inner hair cell under control conditions (black) and after exposure to the SERCA inhibitor t-BHQ (gray). (*D*) Same as in *C*, but for a chicken short hair cell.

25 μM). t-BHQ had no significant effect on outward current decay in rat inner hair cells (decay time constant, 32 ± 3 ms; $P = 0.382$, paired *t* test), but reduced that of chicken hair cells to 74 ± 7 ms ($P = 0.005$, paired *t* test) (Fig. 4 *C* and *D*).

Molecular Evolution of α7 and α4β2 nAChRs. The phylogenetic difference in Ca^{2+} permeability appears as a peculiar feature of the α9α10 nAChR and has not been reported for other nAChRs. For example, Ca^{2+} permeability is at the high end (pCa/pNa, ~10–20) for both mammalian (18, 25, 26) and chicken (27) α7 nAChRs and 10 times lower both for mouse and chicken α4β2 receptors (pCa/pNa, 1.7) (28, 29). Thus, conservation of the molecular bases underlying Ca^{2+} permeability in α7 and α4β2 nAChRs during the evolution of birds and mammals would be expected. To study the evolutionary histories of vertebrate α7, α4, and β2 subunits, we implemented the branch-site test of positive selection, which detects the presence of sites under positive selection within a given gene in specific lineages of a phylogeny (30, 31). This test is based in the comparison of two evolutionary models. The branch-site model (H_A) allows sites in the foreground lineage to evolve under positive selection, whereas in the null model (H_0), sites are allowed to evolve only under either purifying selection ($\omega < 1$) or neutral evolution ($\omega = 1$). We then used a likelihood ratio test (LRT) to assess whether the branch-site model fit the data better than the null hypothesis. Our results (Table 1) indicate that for the genes encoding the α7 (*CHRNA7*), α4 (*CHRNA4*), and β2 (*CHRNB2*) subunits, a model that allows sites to evolve positively in the lineage leading to mammals does not fit the data better than the null hypothesis. For the sake of comparison, we extended our previous analysis of the evolution of *CHRNA10* to include additional species. As shown in Table 1, for *CHRNA10* with mammals as the foreground branch, an LRT value of 9.39 was obtained ($P < 0.0021$), indicating positive selection in this lineage. Conducting the same tests but considering other vertebrate lineages (placental mammals or birds/reptiles) as evolving positively revealed no signatures of positive selection for any of the four genes. In addition, a phylogenetic tree including known vertebrate nAChR subunits from representative species shows that whereas α9, α7, α4, β2, and other nAChR subunits follow the main vertebrate taxa grouping, mammalian α10 subunits form a unique clade separate from other nonmammalian vertebrate α10 subunits that group with α9 subunits (Fig. S3). Thus, as shown in a collapsed phylogenetic tree (Fig. 5), all nAChRs have their individual unique branch, with the exception of α10, which has two separate branches, one for mammals and one for nonmammalian vertebrates. Taken together, these results indicate that, in contrast to the mammalian α10 nAChR subunit, α7, α4, and β2 were not shaped by positive selection and were under purifying selection in all vertebrate species.

Discussion

The ability of Ca^{2+} to perform its various local tasks within the cell depends on steep gradients in concentration encountered in the vicinity of open Ca^{2+}-permeable channels (32). In contrast to voltage-gated Ca^{2+} channels, ligand-gated channels provide Ca^{2+} influx at voltages close to the resting membrane potential, as is the case for nAChRs. Based on their relative Ca^{2+} permeability, nAChRs have been subdivided into three categories that are conserved among vertebrate species. The muscle type is the least permeable of all nAChR family members (pCa/pNa, ~0.2–0.4) (33–35). Heteromeric neuronal receptors have higher Ca^{2+} permeability (pCa/pNa, ~1.5) (19, 35–37), and the homomeric α7 and α8 receptors have the highest relative Ca^{2+} permeability (pCa/pNa, ~10–20) (18, 27). The main finding of the present work is that, in contrast to other nAChRs, the Ca^{2+} permeability of α9α10 nAChRs is not uniform across species. It is unexpectedly low and similar to that of heteromeric neuronal nAChRs in chicken α9α10 nAChRs (present results) and high and similar to that of homomeric α7- and α8-containing receptors in rat α9α10 nAChRs (10, 13, 14). Given that the α10 nAChR subunit has been under strong positive selection in mammals (ref. 12 and present results), we suggest that increased Ca^{2+} permeability might be the functional novelty resulting from that selective pressure. Although some degree of variability in Ca^{2+} permeability exists across species for other nAChRs, the large differences described here for α9α10

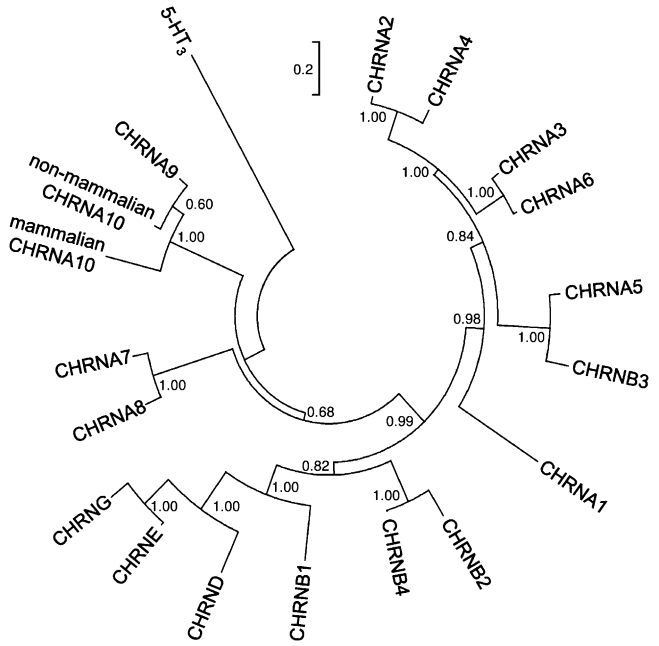

Fig. 5. Phylogenetic tree of nAChR subunits. The tree represents the collapsed phylogenetic relationships among vertebrate nAChR subunits. The branches corresponding to the same subunits of different species were condensed up to the node at which one subunit separates from its closest neighbor. The complete tree is shown in Fig. S3. Numbers in branches indicate the bootstrap value obtained after 1,000 replicates. Note that the α10 subunit is the only one to show two separate branches; nonmammalian α10 subunits are closely related to α9 subunits, whereas mammalian α10 subunits form a separate clade.

nAChRs have not been reported previously (38). Thus, in contrast to the findings for α10, the lack of evidence of positive selection of α7, α4, and β2 nAChR subunits across vertebrate species is in agreement with the observation that Ca^{2+} permeability ratios are conserved as well.

Several lines of evidence pinpoint the pore lining transmembrane region 2 (TM2) of nAChRs as responsible for providing the molecular determinants underlying Ca^{2+} permeability. Thus, mutations at positions −1′, 16′, and 17′ of TM2 (Fig. S4) abolish Ca^{2+} permeability of several nAChR receptors (15, 27). Alignment of the α10 TM2 region of several vertebrate species indicates that all of these residues are highly conserved in mammalian and nonmammalian vertebrates (Fig. S4), precluding their involvement in the observed permeability differences.

Efferent control is a common feature of all vertebrate hair cells (39), and ACh is thought to produce hyperpolarization of hair cells in both mammals and birds (as well as other vertebrates) through the activation of SK Ca^{2+}-dependent K^+ channels (see ref. 9 for a review). Nearby cytoplasmic stores may contribute additional calcium in hair cells (40). Although postsynaptic cisterns are omnipresent features of efferent synapses in auditory hair cells of birds and mammals (23, 24), the relative contributions of calcium influx and store release might vary between chicken and rat hair cells. Compared with rat hair cells, in chicken hair cells, cholinergic activation of calcium-dependent SK channels had a prolonged time course at a voltage at which calcium influx was minimized. This activation was sensitive to SERCA inhibition in chicken hair cells but not in rat hair cells, suggesting that in the former, the postsynaptic calcium signal owes its duration to release from stores. It also suggests that release of calcium from synaptic stores, at least under these experimental conditions, plays a lesser role in rat hair cells, consistent with greater calcium influx through these cells' nAChRs. Of interest, the decay time constant of SK "tail current" in rat hair cells is similar to that reported previously for synaptic currents of inner (41, 42) and outer (11) cochlear hair cells. However, it should be noted that calcium stores might become more important during prolonged cholinergic inhibition of rat cochlear hair cells (40, 43).

Given that the lineages leading to modern birds and mammals separated at least 300 Mya (39, 40), the foregoing results might indicate that independent solutions to functional demands evolved in parallel for the avian basilar papilla and the mammalian cochlea. However, the increasingly calcium-permeable nAChR of rat cochlear hair cells might also indicate that stronger efferent inhibition is required for mammalian cochlear hair cells. It has been observed (44–46) and recently elaborated (47) that OHCs exhibit increasing membrane ionic conductance moving from apical, low-frequency positions to higher-frequency basal locations in the mammalian cochlea. This increased membrane conductance along with decreased capacitance (membrane area) confers shorter membrane time constants to high-frequency basal OHCs. Consequently, the prestin-dependent electromotility that provides cochlear amplification in mammals can extend to acoustic frequencies above 10 kHz (47). Because efferent synaptic inhibition acts as a parallel shunt, the inhibitory conductance must increase with "resting" membrane conductance to remain effective. Thus, larger synaptic contacts in the high-frequency basal region might be expected, as has been reported previously (46). Moreover, the fact that RT-PCR and in situ hybridization measurement of α9 expression shows both longitudinal and radial gradients, with the greatest expression over OHCs in basal regions (48), might indicate a higher density of nAChRs in the high-frequency region of the cochlea. Further inhibitory strength could be gained by increasing the flux of calcium that activates the hyperpolarizing K^+ conductance. The recent report indicating that cholinergic inhibition of basal (high-frequency) rat OHCs specifically uses large-conductance BK channels in addition to the small-conductance SK channels that serve solely in apical OHCs lends additional credence to this hypothesis (46). Thus, it can be conjectured that increased Ca^{2+} permeability helps activate low–Ca^{2+}-affinity, high-conductance BK channels (49) in mammalian basal OHCs, whereas Ca^{2+} influx provided by the nonmammalian nAChR suffices to activate the high–Ca^{2+}-affinity, low-conductance SK channels (49).

In summary, the present work reports a substantial interspecies difference in Ca^{2+} permeability for a nAChR. In addition, it suggests that efferent inhibition of mammalian cochlear hair cells might especially benefit from a cholinergic receptor with enhanced calcium permeability.

Materials and Methods

All experimental protocols were carried out in accordance with National Institutes of Health guidelines for the care and use of laboratory animals, as well as guidelines of the Institutional Animal Care and Use Committees of The Johns Hopkins University and Instituto de Investigaciones en Ingeniería Genética y Biología Molecular.

Expression of Recombinant Receptors in *X. laevis* Oocytes. The plasmids used for heterologous expression in *X. laevis* oocytes are described in *SI Materials and Methods*. Electrophysiological recordings from *Xenopus* oocytes were obtained as described previously (6, 50) and are described in more detail in *SI Materials and Methods*.

Chicken Basilar Papilla. Patch-clamp recordings from short hair cells of the auditory organ (basilar papilla) were obtained as described in *SI Materials and Methods*.

Calcium Permeability. The relative pCa/pMono values were evaluated as done previously for recombinant and native mammalian α9α10 receptors (10, 13, 14, 50), by analyzing the shift in the reversal potential (E_{rev}) as a function of the increase in the extracellular Ca^{2+} concentration and fitting the data to the GHK constant field voltage equation, assuming no anion permeability and extended to include divalent cations (51, 52). A detailed description of the protocol is provided in *SI Materials and Methods*.

Molecular Evolution Analysis. All sequences were downloaded from GenBank and Ensembl databases. Alignments of sequences used for the evolutionary analysis are shown in Fig. S5, and accession numbers are listed in Table S2. To test for the presence of positive selection, the branch-site test of positive selection developed by Yang and coworkers (30, 31) was applied using the codeml program implemented in PAML, as discussed in *SI Materials and Methods*. Phylogenetic trees were built using MEGA4, as described in *SI Materials and Methods*.

ACKNOWLEDGMENTS. This work was supported by the National Institute on Deafness and other Communication Disorders Grant R01DC001508 (to P.A.F. and A.B.E.), an International Research Scholar Grant from the Howard Hughes Medical Institute (to A.B.E.), research grants from the Agencia Nacional de Promoción Científica y Tecnológica and grants from the University of Buenos Aires and the Consejo Nacional de Investigaciones Cientificas y Técnicas (CONICET) (to L.F.F., A.B.E, and E.K.), and the National Research Foundation of Korea Grant NRF-2010-013-E00015 (to G.J.I.). M.L. and F.P. are research fellows at CONICET.

1. Karlin A (2002) Emerging structure of the nicotinic acetylcholine receptors. *Nat Rev Neurosci* 3:102–114.
2. Dent JA (2006) Evidence for a diverse Cys-loop ligand-gated ion channel superfamily in early bilateria. *J Mol Evol* 62:523–535.
3. Le Novère N, Corringer PJ, Changeux JP (2002) The diversity of subunit composition in nAChRs: Evolutionary origins, physiologic and pharmacologic consequences. *J Neurobiol* 53:447–456.
4. Dani JA, Bertrand D (2007) Nicotinic acetylcholine receptors and nicotinic cholinergic mechanisms of the central nervous system. *Annu Rev Pharmacol Toxicol* 47:699–729.
5. Eatock RA, Songer JE (2011) Vestibular hair cells and afferents: Two channels for head motion signals. *Annu Rev Neurosci* 34:501–534.
6. Elgoyhen AB, Johnson DS, Boulter J, Vetter DE, Heinemann S (1994) Alpha 9: An acetylcholine receptor with novel pharmacological properties expressed in rat cochlear hair cells. *Cell* 79:705–715.
7. Elgoyhen AB, et al. (2001) alpha10: A determinant of nicotinic cholinergic receptor function in mammalian vestibular and cochlear mechanosensory hair cells. *Proc Natl Acad Sci USA* 98:3501–3506.
8. Plazas PV, Katz E, Gomez-Casati ME, Bouzat C, Elgoyhen AB (2005) Stoichiometry of the alpha9alpha10 nicotinic cholinergic receptor. *J Neurosci* 25:10905–10912.
9. Elgoyhen AB, Katz E (2011) The efferent medial olivocochlear–hair cell synapse. *J Physiol Paris*, 10.1016/j.jphysparis.2011.06.001.
10. Gómez-Casati ME, Fuchs PA, Elgoyhen AB, Katz E (2005) Biophysical and pharmacological characterization of nicotinic cholinergic receptors in rat cochlear inner hair cells. *J Physiol* 566:103–118.
11. Oliver D, et al. (2000) Gating of Ca^{2+}-activated K^+ channels controls fast inhibitory synaptic transmission at auditory outer hair cells. *Neuron* 26:595–601.
12. Franchini LF, Elgoyhen AB (2006) Adaptive evolution in mammalian proteins involved in cochlear outer hair cell electromotility. *Mol Phylogenet Evol* 41:622–635.
13. Weisstaub N, Vetter DE, Elgoyhen AB, Katz E (2002) The alpha9alpha10 nicotinic acetylcholine receptor is permeable to and is modulated by divalent cations. *Hear Res* 167:122–135.
14. Sgard F, et al. (2002) A novel human nicotinic receptor subunit, alpha10, that confers functionality to the alpha9-subunit. *Mol Pharmacol* 61:150–159.
15. Haghighi AP, Cooper E (2000) A molecular link between inward rectification and calcium permeability of neuronal nicotinic acetylcholine alpha3beta4 and alpha4-beta2 receptors. *J Neurosci* 20:529–541.
16. Fucile S, Sucapane A, Eusebi F (2006) Ca^{2+} permeability through rat cloned alpha9-containing nicotinic acetylcholine receptors. *Cell Calcium* 39:349–355.
17. Boton R, Dascal N, Gillo B, Lass Y (1989) Two calcium-activated chloride conductances in *Xenopus laevis* oocytes permeabilized with the ionophore A23187. *J Physiol* 408: 511–534.
18. Séguéla P, Wadiche J, Dineley-Miller K, Dani JA, Patrick JW (1993) Molecular cloning, functional properties, and distribution of rat brain alpha 7: A nicotinic cation channel highly permeable to calcium. *J Neurosci* 13:596–604.
19. Vernino S, Amador M, Luetje CW, Patrick J, Dani JA (1992) Calcium modulation and high calcium permeability of neuronal nicotinic acetylcholine receptors. *Neuron* 8: 127–134.
20. McNiven AI, Yuhas WA, Fuchs PA (1996) Ionic dependence and agonist preference of an acetylcholine receptor in hair cells. *Aud Neurosci* 2:63–77.
21. Fuchs PA, Murrow BW (1992) Cholinergic inhibition of short (outer) hair cells of the chick's cochlea. *J Neurosci* 12:800–809.
22. Ballestero J, et al. (2011) Short-term synaptic plasticity regulates the level of olivocochlear inhibition to auditory hair cells. *J Neurosci* 31:14763–14774.
23. Hirokawa N (1978) The ultrastructure of the basilar papilla of the chick. *J Comp Neurol* 181:361–374.
24. Saito K (1983) Fine structure of the sensory epithelium of guinea-pig organ of Corti: Subsurface cisternae and lamellar bodies in the outer hair cells. *Cell Tissue Res* 229: 467–481.
25. Fucile S, Palma E, Mileo AM, Miledi R, Eusebi F (2000) Human neuronal threonine-for-leucine-248 alpha 7 mutant nicotinic acetylcholine receptors are highly Ca^{2+} permeable. *Proc Natl Acad Sci USA* 97:3643–3648.
26. Fucile S, Renzi M, Lax P, Eusebi F (2003) Fractional Ca(2+) current through human neuronal alpha7 nicotinic acetylcholine receptors. *Cell Calcium* 34:205–209.
27. Bertrand D, Galzi JL, Devillers-Thiéry A, Bertrand S, Changeux JP (1993) Mutations at two distinct sites within the channel domain M2 alter calcium permeability of neuronal α7 nicotinic receptor. *Proc Natl Acad Sci USA* 90:6971–6975.
28. Lax P, Fucile S, Eusebi F (2002) Ca(2+) permeability of human heteromeric nAChRs expressed by transfection in human cells. *Cell Calcium* 32:53–58.
29. Ragozzino D, Barabino B, Fucile S, Eusebi F (1998) Ca^{2+} permeability of mouse and chick nicotinic acetylcholine receptors expressed in transiently transfected human cells. *J Physiol* 507:749–757.
30. Yang Z, Nielsen R (2002) Codon-substitution models for detecting molecular adaptation at individual sites along specific lineages. *Mol Biol Evol* 19:908–917.
31. Zhang J, Nielsen R, Yang Z (2005) Evaluation of an improved branch-site likelihood method for detecting positive selection at the molecular level. *Mol Biol Evol* 22: 2472–2479.
32. Simon SM, Llinás RR (1985) Compartmentalization of the submembrane calcium activity during calcium influx and its significance in transmitter release. *Biophys J* 48: 485–498.
33. Adams DJ, Dwyer TM, Hille B (1980) The permeability of endplate channels to monovalent and divalent metal cations. *J Gen Physiol* 75:493–510.
34. Decker ER, Dani JA (1990) Calcium permeability of the nicotinic acetylcholine receptor: The single-channel calcium influx is significant. *J Neurosci* 10:3413–3420.
35. Vernino S, Rogers M, Radcliffe KA, Dani JA (1994) Quantitative measurement of calcium flux through muscle and neuronal nicotinic acetylcholine receptors. *J Neurosci* 14:5514–5524.
36. Fieber LA, Adams DJ (1991) Acetylcholine-evoked currents in cultured neurones dissociated from rat parasympathetic cardiac ganglia. *J Physiol* 434:215–237.
37. Sands SB, Barish ME (1992) Neuronal nicotinic acetylcholine receptor currents in phaeochromocytoma (PC12) cells: Dual mechanisms of rectification. *J Physiol* 447: 467–487.
38. Fucile S (2004) Ca^{2+} permeability of nicotinic acetylcholine receptors. *Cell Calcium* 35: 1–8.
39. Köppl C (2011) Birds—Same thing, but different? Convergent evolution in the avian and mammalian auditory systems provides informative comparative models. *Hear Res* 273:65–71.
40. Lioudyno M, et al. (2004) A "synaptoplasmic cistern" mediates rapid inhibition of cochlear hair cells. *J Neurosci* 24:11160–11164.
41. Glowatzki E, Fuchs PA (2000) Cholinergic synaptic inhibition of inner hair cells in the neonatal mammalian cochlea. *Science* 288:2366–2368.
42. Katz E, et al. (2004) Developmental regulation of nicotinic synapses on cochlear inner hair cells. *J Neurosci* 24:7814–7820.
43. Sridhar TS, Brown MC, Sewell WF (1997) Unique postsynaptic signaling at the hair cell efferent synapse permits calcium to evoke changes on two time scales. *J Neurosci* 17: 428–437.
44. Mammano F, Ashmore JF (1996) Differential expression of outer hair cell potassium currents in the isolated cochlea of the guinea-pig. *J Physiol* 496:639–646.
45. Ricci AJ, Crawford AC, Fettiplace R (2003) Tonotopic variation in the conductance of the hair cell mechanotransducer channel. *Neuron* 40:983–990.
46. Wersinger E, McLean WJ, Fuchs PA, Pyott SJ (2010) BK channels mediate cholinergic inhibition of high-frequency cochlear hair cells. *PLoS ONE* 5:e13836.
47. Johnson SL, Beurg M, Marcotti W, Fettiplace R (2011) Prestin-driven cochlear amplification is not limited by the outer hair cell membrane time constant. *Neuron* 70: 1143–1154.
48. Simmons DD, Morley BJ (1998) Differential expression of the alpha 9 nicotinic acetylcholine receptor subunit in neonatal and adult cochlear hair cells. *Brain Res Mol Brain Res* 56:287–292.
49. Fakler B, Adelman JP (2008) Control of K(Ca) channels by calcium nano/microdomains. *Neuron* 59:873–881.
50. Katz E, et al. (2000) High calcium permeability and calcium block of the alpha9 nicotinic acetylcholine receptor. *Hear Res* 141:117–128.
51. Lewis CA (1979) Ion-concentration dependence of the reversal potential and the single channel conductance of ion channels at the frog neuromuscular junction. *J Physiol* 286:417–445.
52. Jan LY, Jan YN (1976) L-glutamate as an excitatory transmitter at the *Drosophila* larval neuromuscular junction. *J Physiol* 262:215–236.